Toward Reconciling STEM and SAXS Data from Ionomers by Investigating Gold Nanoparticles

Nicholas M. Benetatos,[†] Brian W. Smith,[†,§] Paul A. Heiney,[‡] and Karen I. Winey[*,†]

Department of Materials Science and Engineering and Department of Physics and Astronomy, University of Pennsylvania, Philadelphia, Pennsylvania 19104-6272

Received June 30, 2005; Revised Manuscript Received August 15, 2005

ABSTRACT: To date, the sizes of the nanoscale ionic aggregates present in ionomers as determined by scanning transmission electron microscopy (STEM) experiments are inconsistent with small-angle X-ray scattering (SAXS) data interpreted by the Yarusso−Cooper model. To address this discrepancy, we have investigated a pair of model nanoparticles (11- and 55-atom Au clusters) with both STEM and SAXS. To mimic ionic aggregates, these nanoparticles were supported by amorphous PS films of predetermined thickness. While the size of the STEM probe was inconsequential to the resolution and measurement of the particles, the optimal specimen thickness was determined to be less than 50 nm. SAXS was performed on dilute solutions of the nanoparticles and fit using a monodisperse, noninteracting hard-sphere form factor model. For Au 11, STEM finds a diameter of 1.3 ± 0.14 nm and SAXS finds a diameter of 1.4 nm. Similarly, both STEM and SAXS determine a diameter of 1.7 nm for Au 55. For a combined system of Au 11 and Au 55, STEM data suggests a bimodal distribution of particle sizes consistent with those of the individual particles while SAXS data indicate hard spheres with diameter of 1.6 nm. Analysis of this model system has allowed us to optimize several experimental conditions of potential importance in reconciling STEM and SAXS data from ionomers.

Introduction

Ionomers are copolymers in which a small fraction (<10%) of the monomeric units contain ionic functional groups. Because of their exceptional chemical and physical properties, these materials have found application in a diverse spectrum of areas including coatings, packaging, and ion-transport membranes. As a result, the structure−processing−property relationships of ionomers have attracted increasing attention in the polymer community. The remarkable properties of ionomers can be attributed to the assembly of ionic functional groups and counterions into nanometer scale ionic aggregates which act as transient physical cross-links. For years, the nanometer scale morphology of ionomers has been studied using small-angle X-ray scattering (SAXS), and the interpretation of these data has evolved through a variety of controversial scattering models.[1] Of these models, the most widely accepted is the Yarusso−Cooper model which has predicted the sizes and spacing between ionic aggregates for a variety of systems including poly(ethylene-*ran*-methacrylic acid) (EMAA) and poly(styrene-*ran*-sulfonated styrene) (SPS) ionomers.[2,3] This modified hard-sphere scattering model has shown that the diameter of the ionic aggregates can vary significantly as a function of main chain characteristics ranging from ∼2.0 nm in the SPS system to 0.8 nm for EMAA ionomers. In these scattering studies, the choice of neutralizing counterion was not observed to impact the ionic aggregate size.

Recently, the use of scanning transmission electron microscopy (STEM) has emerged as a powerful tool for the nanometer scale characterization of ionomers.[4] This technique provides high-resolution imaging capability with contrast generated by differences in atomic number (Z). In STEM, a convergent beam of electrons is focused into an ultrafine point called the STEM probe, which is subsequently rastered across the specimen. The electrons are transmitted through the specimen en route to the STEM bright field (BF) detector positioned directly below. When an area of increased local average Z is encountered by the probe, the electrons are elastically scattered to high angles and do not hit the BF detector. Thus, in BF STEM images, the nanometer-sized areas of increased average atomic number appear dark against a brighter background corresponding to lighter elements. Alternatively, the electrons scattered to high angle may be detected using a high angle annular dark field (HAADF) detector. In this case, the HAADF STEM images depict areas of increased average atomic number as bright regions amidst a dark background because electrons scattered at small angles (i.e., by lower Z regions) pass through the annular detector.

These unique imaging capabilities of STEM have led to the first direct visualization of the ionic aggregates in thin specimen microtomed from bulk ionomers.[5] The advantage of this method lies in the ability to assess the size, shapes, and spatial distribution of the ionic aggregates directly, without the use of any models, while preserving the bulk morphology of the material. In contrast to the SAXS data interpreted by the Yarusso−Cooper model, STEM experiments have found the diameter of the ionic aggregates in EMAA ionomers neutralized with zinc counterions to be on the order of 2.1 nm—more than 2-fold larger than measured by SAXS. In addition to this size discrepancy, other STEM studies have revealed a heterogeneity in morphology with changes in the choice of both neutralizing counterion and polymer backbone.[6−8] These results have led to increased curiosity regarding how ionomer morphologies change as a function of materials chemistry and processing. Although the field has seen extensive re-

[†] Department of Materials Science and Engineering.
[‡] Department of Physics and Astronomy.
[§] Current address. Department of Medical Oncology, Fox Chase Cancer Center, Philadelphia, PA.
* To whom correspondence should be addressed.

10.1021/ma051419i CCC: $30.25
Published on Web 09/30/2005

search efforts, a complete description of the structure−processing−property relationships in ionomers has remained elusive.

Despite the many advantages offered by STEM, the applicability of this technique is somewhat limited by the specimen preparation process. To obtain interpretable STEM data, the specimen must be stable and appropriately electron transparent. Depending on the material under investigation, the length scale of the relevant structural features, and the microscope, the appropriate specimen thickness can vary appreciably. In the characterization of soft materials, bulk samples are typically sliced into thin specimen using an ultramicrotome equipped with a diamond knife. The thickness of sections ranging between ~90 and 200 nm may be estimated due to changes in color which result from the interference of visible light. However, it is a significant challenge to determine the thickness of sections thinner than 50 nm. In the case of high-resolution STEM imaging of ionomers, in which there is considerable debate as to the size of the ionic aggregates, it is necessary to establish the optimal conditions, especially section thickness, under which the most accurate depiction of the nanoscale morphology may be determined.

Here we investigate factors of central importance in the characterization of ionomers by STEM. Because of the large variability observed in ionomer morphologies as a function of chemistry and processing, we have chosen to model the ionic aggregates using Au nanoparticles. These commercially available particles have found application as electron microscopy labels in biological systems and have been featured in several studies.[9−11] The size of the Au nanoparticles is similar to that of the ionic aggregates in ionomer systems, and the high atomic number of gold ($Z = 79$) makes the system ideal for characterization by both STEM and SAXS. By depositing these particles atop spin-cast polystyrene films of predetermined thickness, the effect of STEM specimen thickness was explored in a controlled manner. This model system also offers the capability of reconciling STEM and SAXS data on length scales comparable to those relevant in the study of ionomer morphology while at the same time offering alternative methods for the determination of nanoscale particle size.

Experimental Section

Eleven-atom and 55-atom gold cluster complexes were purchased from Nanoprobes Inc., Yaphank, NY. Upon receipt of these solids, dilute solutions were prepared from methanol and characterized by dynamic light scattering, UV−vis spectroscopy, STEM, and SAXS. All raw materials were stored at −20 °C, while methanol solutions were refrigerated and maintained at 4 °C.

Dynamic light scattering measurements were performed with a Malvern Zetasizer NanoS spectrometer, equilibrated at 25 °C, using a 633 nm laser. To minimize dust contamination, each sample was passed through a PVDF syringe filter (220 nm pore size) directly into a clean and dry quartz cuvette. Data from multiple independent measurements were collected over several hours. The number-weighted mean diameter of the 11- and 55-atom gold nanoparticles was measured to be 2.1 and 2.6 nm, respectively. This diameter includes both the Au core and the surrounding organic stabilizing ligands.

Absorbance measurements were performed using a Varian instruments Cary 5000 spectrophotometer. Data were acquired by scanning at 1 nm increments over the range between 200 and 900 nm. The absorbance spectrum of Au 11 shows sharper, better defined peaks than that of Au 55. This is consistent with the expectation that the smaller number of atoms in the Au 11 cluster should result in narrower energy bands and therefore more molecular optical behavior.

Polystyrene films were spin-cast (2000 rpm, 60 s) from solutions (0.5−2.0% PS by weight) onto clean Si substrates. The film thickness was measured by ellipsometry. Films were then floated onto distilled ultrafiltered water, collected atop Cu TEM grids, and dried under vacuum. 5 μL aliquots of Au nanoparticle solutions (methanol) were deposited onto the PS films and allowed to stand for 3 min. Excess solution was then removed using filter paper. All grids containing the Au particles were stored under vacuum prior to STEM experiments.

STEM experiments were performed on a JEOL 2010F field emission electron microscope operated at 197 kV with a 70 μm condenser aperture. Images (512 × 512 pixels) were acquired using a Gatan high-angle annular dark field (HAADF) scintillating detector with linear intensity response and collection angle ranging between 50 and 115 mRAD. Magnifications ranged from 300 000 times (300k×) to 3 000 000 times (3000k×). Measurements via Scion Image software were performed on multiple, unenhanced, digital images at a magnification of 3000k×, with a pixel size of 0.075 nm. For presentation, postanalysis image enhancement was performed with Adobe Photoshop 5.0 using standard techniques including gray level adjustment and brightness/contrast manipulation. These enhancements were applied uniformly to entire images.

1 mM methanol solutions of Au 11 and Au 55 for small-angle X-ray scattering (SAXS) were injected into glass capillary tubes (3, 5 mm diameter) via syringe, and the tubes were subsequently sealed. SAXS experiments were carried out in our multiple angle X-ray scattering (MAXS) facility, which consists of a Nonius FR591 rotating-anode generator operated at 40 kV × 85 mA, mirror−monochromator focusing optics, an evacuated flight path, and a Bruker HiSTAR multiwire two-dimensional detector. Data were acquired over a 1 h interval at a sample−detector distance of 11 cm. Isotropic, two-dimensional data were integrated azimuthally over 180° to yield I vs q data. Data analysis and curve fitting were performed using Datasqueeze software.

Results and Discussion

STEM of Au 11 and Au 55. Using HAADF−STEM, we have imaged the cores of both Au 11 and Au 55 gold cluster complexes deposited on 20 nm thick PS substrates (Figure 1). The bright spots visible in these HAADF STEM images correspond to particle cores of higher average atomic number (Au) compared to the surrounding polymer substrate and the predominantly hydrocarbon ligand shell. The differences in intensity which are occasionally observed between particles of similar size can be attributed to the presence of particles both above and below the PS film. Upon observation of these images, it is qualitatively evident that Au 55 appears slightly larger and more polydisperse than Au 11.

The size determination of isolated objects present in digital images may be performed a number of ways. To reproducibly measure the size of these particles with minimum error, we have adopted the following method. A line of pixels is scanned across the image of an isolated particle (Figure 2, inset), and the intensity level is recorded for each pixel. A Gaussian curve is fit to the profile, and the fwhm of this curve is taken as the particle diameter. Figure 2 illustrates the line intensity profile of an Au 11 particle fit with a Gaussian curve of fwhm = 1.4 nm. Each point in the intensity profile represents the gray scale intensity level at each pixel along the line, where pixels have been converted to distance. This method allows for a systematic and easily reproduced measurement of large numbers of particles

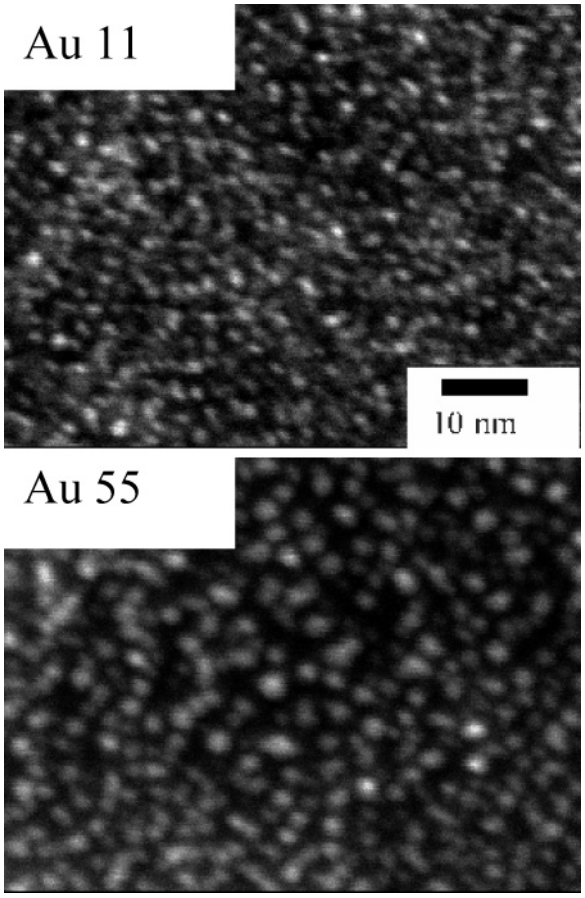

Figure 1. HAADF STEM images of Au 11 and Au 55 gold cluster complexes deposited on 20 nm PS substrates. Qualitatively, Au 55 appears larger and more polydisperse compared to Au 11. STEM images collected at 1200k× with a 0.7 nm STEM probe.

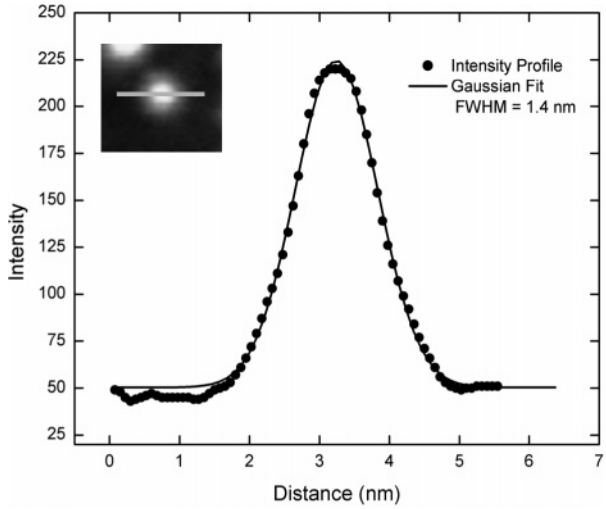

Figure 2. STEM intensity profile of a single Au 11 particle and Gaussian fit. Data points represent the gray scale intensity at each pixel along a line approximated by the segment shown (inset).

without the arbitrary assignment of particle boundaries. To obtain the most accurate measurement, the pixel size must be small compared to that of the object. It is therefore imperative that the images are acquired under high-resolution conditions at magnifications on the order of 3000k× where 1 pixel corresponds to 0.075 nm. Without these high magnifications, the number of points per intensity profile is reduced, and the curve fitting becomes less reliable. Measuring the particles in this manner, we have used STEM to determine the average diameter of Au 11 ($D_{\text{STEM Au 11}}$) to be 1.3 ± 0.14 nm and $D_{\text{STEM Au 55}}$ = 1.7 ± 0.25 nm, where the reported value is the mean of >50 particle diameters and the error is the standard deviation of these measurements. The slightly increased polydispersity of Au 55 is evident in the larger standard deviation of the Au 55 particles.

To assess the role of specimen thickness in the resolution and accurate measurement of nanometer scale objects using high resolution STEM, we have imaged and measured the Au 11 particles on PS substrates of thickness ranging between 20 and 90 nm, where the film thickness was measured by ellipsometry. The images of Figure 3 clearly illustrate improved image quality as the specimen thickness is decreased below 50 nm under identical imaging conditions. As thickness increases, the signal of electrons scattered by the Au particles is attenuated prior to detection due to multiple elastic and inelastic scattering events as the electrons travel through the substrate. The result is a decreased signal-to-noise ratio which significantly reduces the quality of the image and the overall sharpness of the features. In addition to the decrease in image quality, thicker PS substrates exhibit a greater tendency to tear upon electron irradiation due to increased inelastic processes. Thermal drift due to phonon oscillations and beam damage were also observed to be more prevalent in thicker specimen. The combination of tearing, drift, and beam damage observed in specimens thicker than 50 nm makes it increasingly difficult to acquire the high-resolution images necessary for accurate measurement of nanoscale particle size. Figure 4 and Table 1 illustrate the considerable variability in measured particle diameter as substrate thickness is increased above 50 nm and the increased standard deviation present in the measurements.

The size of the convergent electron beam probe is also a relevant parameter in the investigation of nanoscale morphologies using high-resolution STEM. We have evaluated the impact of decreasing the STEM probe size by imaging Au 11 particles deposited on PS films with both 0.7 and 0.3 nm probes (Table 1). By using a smaller STEM probe, we do not influence the measured particle size. Images acquired with the 0.3 nm probe show only a decrease in signal intensity due to lower beam current compared with those acquired using a larger STEM probe (0.7 nm). This result suggests that the size of the Au 11 particles is sufficiently large compared to the 0.7 nm probe to obtain images which accurately represent the nanoparticles under these conditions. On the basis of this finding, it is not likely that any probe convolution effects due to size similarity between the probe and the object are relevant in this system.

SAXS of Au 11 and Au 55. Small-angle X-ray scattering was also employed to determine the size of the Au cores for Au 11 and Au 55. Solutions (1 mM in methanol) of these particles sealed inside glass capillaries showed isotropic scattering in the angular range between 1.4 and 6 nm^{-1}. Analysis of a sealed capillary containing only methanol showed no scattered intensity in this region. The system was modeled as monodisperse, noninteracting, hard-sphere scatterers distributed randomly in solution. At a concentration of 1 mM, the average solution volume available for each particle (~1500 nm^3) is large compared to the volume occupied

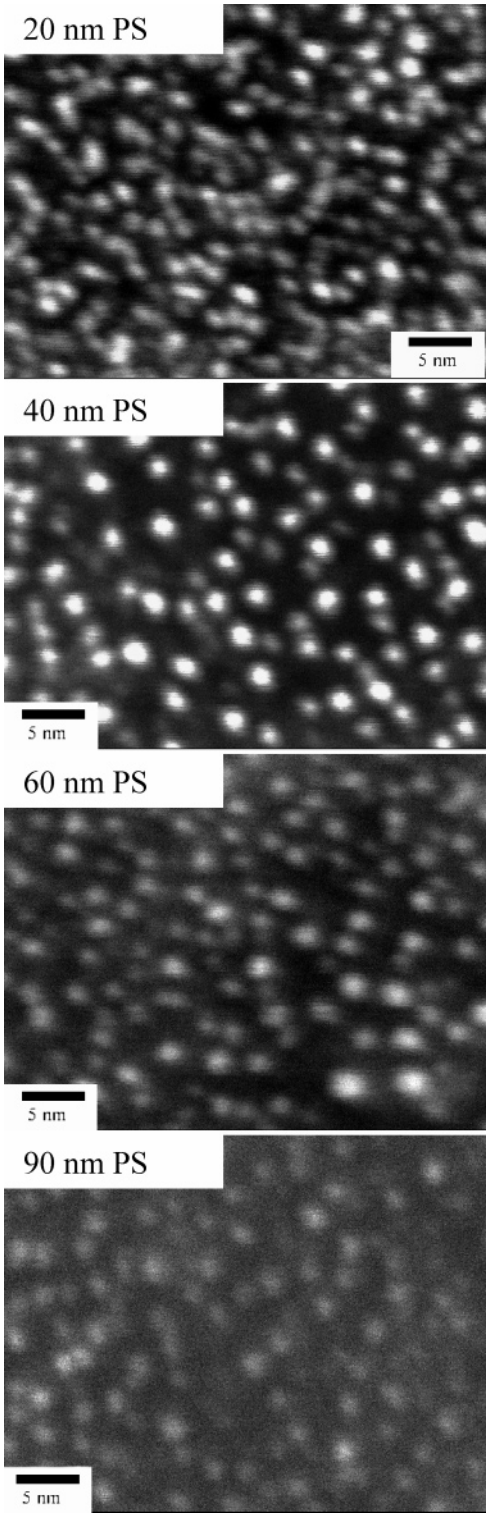

Figure 3. HAADF STEM images depict the effect of increasing specimen thickness from 20 to 90 nm. Image quality decreases significantly at thickness in excess of 50 nm. STEM images collected at 3000k× with a 0.7 nm STEM probe.

by each particle (∼11 nm^3). Under these conditions, interparticle scattering is negligible, and the total scattered intensity is given by the following form factor:

$$I(q) = \left(\frac{3(\sin(qr) - (qr)\cos(qr))}{(qr)^3}\right)^2$$

where r is the hard-sphere radius of the particle.[12] An

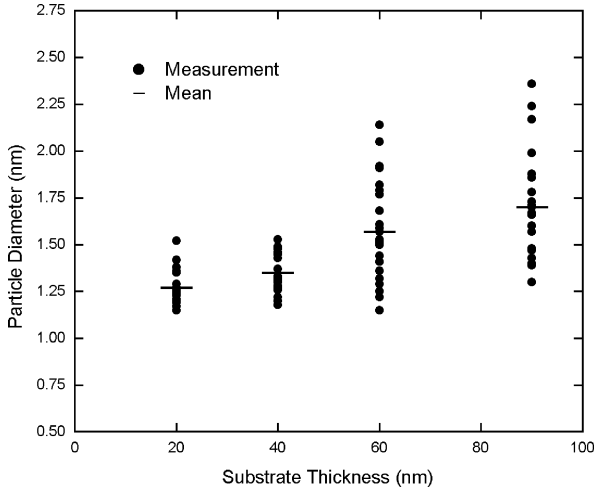

Figure 4. Diameters of Au 11 particles as a function of specimen thickness, where each point is a separate measurement and the horizontal bars indicate the means. Individual measurements were made at each specimen thickness. As substrate thickness exceeds 50 nm, mean values increase and measurements become less accurate.

Table 1. Particle Diameters (nm) and Standard Deviations of Au 11 Measured by STEM

	PS substrate thickness (nm)			
STEM probe (nm)	20	40	60	90
0.3	1.3 ± 0.14	1.4 ± 0.14	1.6 ± 0.28	*a*
0.7	1.3 ± 0.14	1.4 ± 0.14	1.6 ± 0.26	1.7 ± 0.31

[a] Unable to be determined due to significant attenuation of signal.

arbitrary scaling factor was included in the model along with a constant term to account for the experimental scattered intensity. Figure 5A,B depicts the scattered intensity fit to this model for both Au 11 and Au 55. To determine the hard-sphere diameter, a least-squares regression was performed which optimized all fitting parameters of the model and generated the best fit curves. Using this method, the best fit hard-sphere diameters $D_{\text{SAXS Au 11}}$ and $D_{\text{SAXS Au 55}}$ were determined to be 1.4 and 1.7 nm, respectively. In each case, the chi squared parameter which represents how well the model fits the SAXS data was approximately equal to 1. To investigate the sensitivity of this method in determining nanometer scale particle size, we altered the hard-sphere radius by ±0.1 nm and performed regressions with the radius fixed at this slightly different value. The resulting best fit curve no longer accurately fit the SAXS data, and the corresponding chi squared value increased to ∼15. Thus, we have used SAXS to determined the diameter of nanometer scale particles to within very small errors (∼0.2 nm). Note that SAXS should be the preferred characterization method over traditional light scattering when the nanoparticle diameter is <2 nm.

STEM and SAXS of a Mixture of Au 11 and Au 55. A combined system of Au 11 and Au 55 particles has also been investigated by both STEM and SAXS in the same manner as the individual particle systems reported above (Figure 5C,D). The best fit hard-sphere scattering model finds a diameter of 1.6 nm with chi squared of ∼3. Evidently, the simple SAXS model for monodisperse spheres described above is unable to make the distinction between the two individual particles and returns a single hard-sphere diameter which is nearly the mean of the D_{SAXS} values of Au 11 and Au 55. In

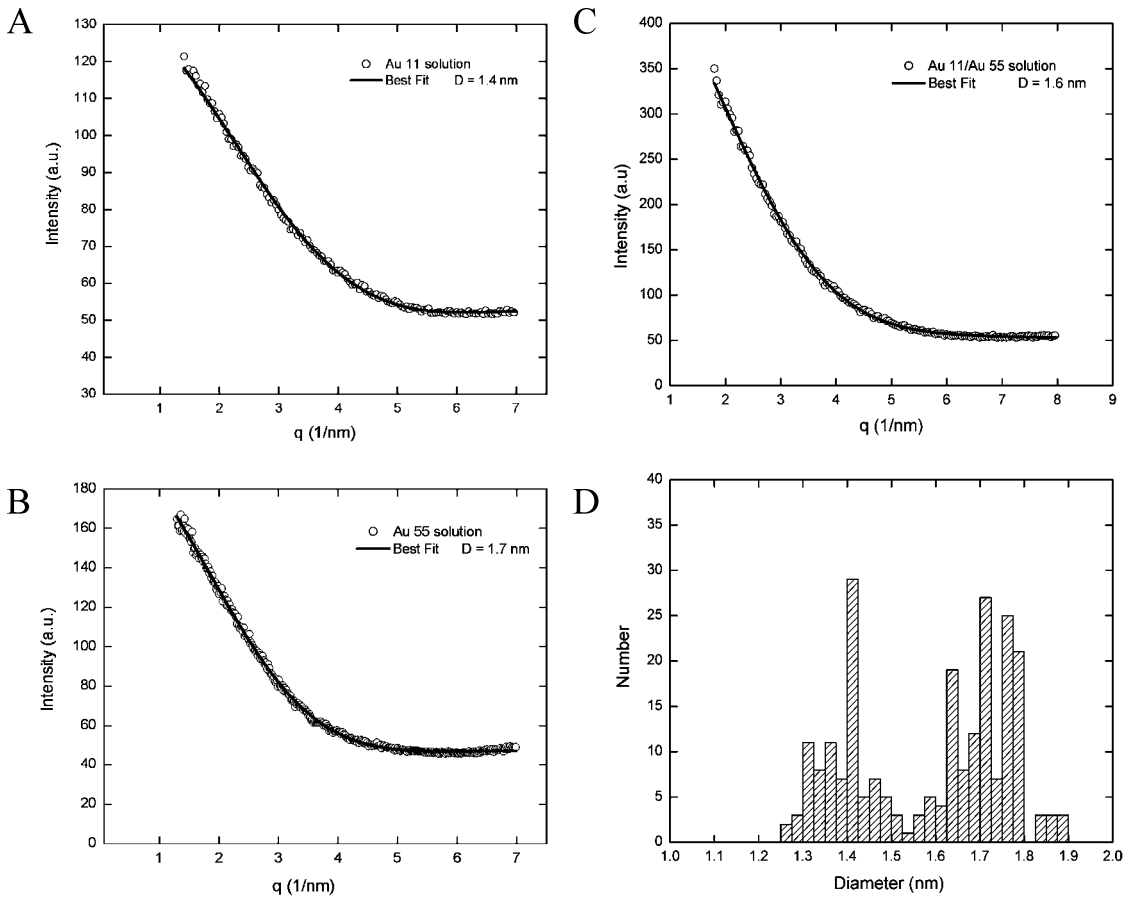

Figure 5. SAXS data and form factor model for solutions of (A) Au 11, (B) Au 55, and (C) a mixture of Au 11 and Au 55. (D) Size distribution histogram for the combined Au 11/Au 55 system as measured by STEM.

the case of the mixed system, STEM measurements suggest a bimodal size distribution in which the sizes and dispersities are consistent with the values of $D_{\text{STEM Au 11}}$ and $D_{\text{STEM Au 55}}$ measured from the individual particle systems. These data clearly highlights the advantage of using STEM to directly determine particle size in more complex nanoparticle systems that cannot accurately be described by simple scattering models without prior knowledge of the particle sizes and relative concentrations.

Comparison of Our STEM and SAXS Particle Size Data. At this point, it is important to clarify the relationship between the particle diameter measured using STEM and that obtained from the SAXS data when modeled as hard spheres. Here, we model the particles as hard spheres in STEM and compare the theoretical intensity profile with the experimentally obtained intensity profiles of the nanoparticles. In the case of a hard-sphere particle, the intensity profile across a 2D projection of a sphere may be calculated in a straightforward manner and is given by

$$I(x) = 2x \tan[\cos^{-1}(x/r)]$$

where r is the radius of the hard sphere and x is the scan distance. The experimental intensity profile from STEM is a convolution of the STEM probe (i.e., a Gaussian with fwhm equal to the probe size) and the intensity profile of the particle, $I(x)$. Figure 6 illustrates the intensity profile of a hard sphere $I(x)$, the convolution of this profile with the 0.7 nm STEM probe, and a Gaussian curve fit to the convolution result. The fwhm

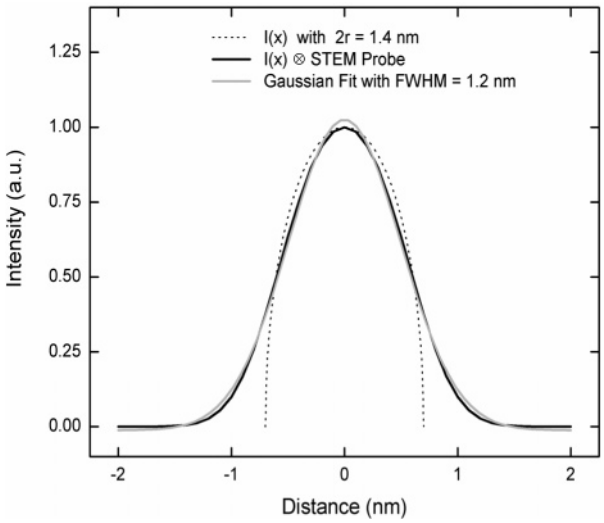

Figure 6. Line scan of the 2D projected intensity for a hard sphere (D = 1.4 nm), the theoretical STEM intensity profile, and the Gaussian fit to the theoretical STEM profile (fwhm = 1.2 nm). The theoretical STEM profile is the convolution of the projected hard-sphere function, $I(x)$, and the 0.7 nm STEM probe.

of the Gaussian curve fit to the theoretical STEM profile of a 1.4 nm hard sphere is 1.2 nm. It is evident that this fwhm slightly underestimates the hard-sphere diameter, although the variation in particle size measured from STEM ($D_{\text{STEM Au 11}} = 1.3 \pm 0.14$ nm) outweighs this slight inconsistency inherent in the measurement process. Thus, the particle sizes determined by STEM and SAXS can be directly compared and are

equivalent to within the experimental error of the two techniques.

Comparison with Particle Size Data from the Literature. Here we compare the sizes we have determine experimentally with diameters predicted by theory as well as available size data for similar particles. Theoretically, the smallest possible gold nanoparticle in which the atoms exhibit fcc packing consists of one central gold atom surrounded by 12 nearest neighbors. On the basis of the lattice parameter of bulk fcc gold (0.407 nm), this theoretical 13-atom crystalline particle has a diameter = 0.864 nm. If another layer of closed-packed atoms is present, the total number of atoms increases from 13 to 55. The theoretical diameter of a 55-atom gold nanoparticle with fcc structure is 1.44 nm. Our STEM measurements have determined the diameter of Au 55 to be 1.7 nm ± 0.25. This number agrees with the size predicted for a 55-atom fcc nanoparticle to within the error of the measurements. However, the diameters we determined by STEM and SAXS for Au 11 ($D_{\text{STEM Au 11}} = 1.3 \pm 0.14$ nm and $D_{\text{SAXS Au 11}} = 1.4$ nm) are larger than the theoretical predictions for fcc nanoparticles. This apparent discrepancy warrants a more detailed discussion.

In the case of Au 11, it should be noted that in addition to the smaller number of atoms (11 vs 13) the particle studied here is not a crystalline fcc nanoparticle but rather an organometallic cluster complex encased in a triarylphosphine ligand shell. This water-soluble Au cluster, originally prepared by Bartlett et al. in 1978, was observed using STEM (pixel size ~ 0.25 nm) by Wall et al. in 1982.[13,14] Their STEM study did not provide a detailed measurement of the particle size, but rather focused on the observation and the utility of these nanoparticles as electron microscopy labels in biological systems. A rigorous structural characterization of the Au clusters by X-ray diffraction was reported by McPartlin et al. in 1969 for a polynuclear Au complex prepared by similar, but not identical, methods.[15] McPartlin et al. collected X-ray diffraction from ordered assemblies of the organometallic cluster complexes. Their diffraction data suggests a Au core having a central Au atom coordinated to 10 adjacent Au atoms at an average distance of 0.267 nm and a total Au core diameter of 0.801 nm.

The particles studied here consist of an 11-atom Au core surrounded by a ligand shell that acts as a particle stabilizer to prevent agglomeration in solution. In the structure provided by the manufacturers, there is one central Au atom and 10 shell Au atoms. Seven of the 10 outer atoms are bonded to a phosphorus atom (Z = 15) at the base of the triarylphosphine ligands, and the remaining three Au atoms are bonded to chlorine (Z = 17) atoms. Unlike McPartlin et al., our morphological investigations were performed on isolated organometallic cluster complexes. Our STEM and SAXS methods probe the local atomic number and local electron density, respectively, and therefore detect both the Au core and the adjacent P and Cl atoms. An estimate of this total diameter is ~1.2 nm, which is the sum of the Au core (0.8 nm, according to McPartlin et al.) and the contribution from the P and Cl atoms (~0.4 nm, twice the atomic diameter). This estimate agrees with the data reported above where $D_{\text{STEM Au 11}} = 1.3 \pm 0.14$ nm and $D_{\text{SAXS Au 11}} = 1.4$ nm. By using the theoretical fcc Au nanoparticle diameter (1.44 nm), we estimate the total diameter of the electron dense region in our Au 55 to be 1.64 nm. This diameter also agrees with our data: $D_{\text{STEM Au 55}} = 1.7 \pm 0.25$ nm and $D_{\text{SAXS Au 55}} = 1.7$ nm.

Conclusion

We have obtained complementary size information from an imaging method (STEM) and a scattering method (SAXS) for a pair of monodisperse, nanometer-scale gold particles, Au 11 and Au 55. Thinner STEM specimens improve the signal-to-noise ratio in images, reduce beam damage, and enable imaging at higher magnifications because there are fewer inelastic scattering events. Furthermore, the observed size of Au nanoparticles increases when the PS support films were larger than 50 nm due to secondary scattering. Using thinner PS support films, STEM imaging can more readily be accomplished at high magnifications and correspondingly small pixel sizes, so that there are numerous points in the intensity profiles across isolated particles. These line scans are fit with Gaussian functions, and we determined that the fwhm of these Gaussian functions correspond well with the diameter of a spherical particle. This analysis method is more reliable than arbitrarily estimating the boundary between the high atomic number particle and the surrounding material.

SAXS is a valuable tool in determining nanoscale particle sizes below the limits of traditional light scattering techniques. We used a form factor scattering model to interpret the SAXS data from a dilute solution and to provide the sphere diameter of the Au nanoparticles. Diameters determined by STEM and SAXS are in strong agreement, demonstrating the quality of the data and data analysis. Finally, when the nanoparticle size distribution is bimodal, as is the case for a mixture of Au 11 and Au 55, the real space imaging method (STEM) has a clear advantage over SAXS.

The ion-rich aggregates in ionomers are comparable in size to the Au nanoparticles studied here. Nanoparticles imaged by TEM or STEM are typically supported by ultrathin support films or attached to holey support films. In contrast, we imaged the nanoparticles on relatively thick PS films, so as to mimic ionomer specimens prepared by ultramicrotomy. The fact that the nanoparticle diameters determined by STEM when the particles were supported on a 20−40 nm thick PS film and by SAXS are consistent demonstrates that it will be possible to reconcile sizes of ionic aggregates using these methods assuming the availability of a suitable scattering model. This paper highlights the importance of specimen thickness and provides renewed confidence as we move toward quantitatively reconciling STEM and SAXS for ionomers.

Acknowledgment. Funding was provided by the National Science Foundation (DMR02-35106). We acknowledge Prof. Russell Composto for the use of the ellipsometer, Prof. David Luzzi for the use of the particle size analyzer and UV−vis spectrometer, and Dr. Doug Yates of the PENN Regional Nanotechnology Facility for helpful discussions and technical assistance with the JEOL 2010F. Nicholas M. Benetatos acknowledges funding provided through the Augustus T. Ashton fellowship at the University of Pennsylvania.

References and Notes

(1) Eisenberg, A.; Kim, J.-S. *Introduction to Ionomers*; John Wiley & Sons: New York, 1998.

(2) Yarusso, D.; Cooper, S. L. *Macromolecules* **1983**, *16*, 1871−1880.
(3) Yarusso, D.; Cooper, S. L. *Polymer* **1985**, *26*, 371−378.
(4) Winey, K. I.; Laurer, J. H.; Kirkmeyer, B. P. *Macromolecules* **2000**, *33*, 507−513.
(5) Laurer, J. H.; Winey, K. I. *Macromolecules* **1998**, *31*, 9106−9108.
(6) Taubert, A.; Winey, K. I. *Macromolecules* **2002**, *35*, 7419−7426.
(7) Kirkmeyer, B. P.; Weiss, R. A.; Winey, K. I. *J. Polym. Sci., Part B: Polym. Phys.* **2001**, *39*, 477−483.
(8) Kirkmeyer, B. P.; Taubert, A.; Kim, J.-S.; Winey, K. I. *Macromolecules* **2002**, *35*, 2648−2653.
(9) Hainfeld, J. F.; Powell, R. D. *J. Histochem. Cytochem.* **2000**, *48*, 471−480.
(10) Hainfeld, J. F.; Furuya, F. R. *J. Histochem. Cytochem.* **1992**, *40*, 177−184.
(11) Schwartz, M. P.; Matouschek, A. *Proc. Natl. Acad. Sci. U.S.A.* **1999**, *96*, 13086−13090.
(12) Guinier, A.; Fournet, G. *Small Angle Scattering of X-rays*; John Wiley: New York, 1955.
(13) Bartlett, P. A.; Bauer, B.; Singer, S. J. *J. Am. Chem. Soc.* **1978**, *100*, 5085−5089.
(14) Wall, J. S.; Hainfeld, J. F.; Bartlett, P. A.; Singer, S. J. *Ultramicroscopy* **1982**, *8*, 397−402.
(15) McPartlin, M.; Mason, R.; Malatesta, L. *Chem. Commun.* **1969**, 334.

MA051419I